

PCCP

Accepted Manuscript



This is an *Accepted Manuscript*, which has been through the Royal Society of Chemistry peer review process and has been accepted for publication.

Accepted Manuscripts are published online shortly after acceptance, before technical editing, formatting and proof reading. Using this free service, authors can make their results available to the community, in citable form, before we publish the edited article. We will replace this *Accepted Manuscript* with the edited and formatted *Advance Article* as soon as it is available.

You can find more information about *Accepted Manuscripts* in the [Information for Authors](#).

Please note that technical editing may introduce minor changes to the text and/or graphics, which may alter content. The journal's standard [Terms & Conditions](#) and the [Ethical guidelines](#) still apply. In no event shall the Royal Society of Chemistry be held responsible for any errors or omissions in this *Accepted Manuscript* or any consequences arising from the use of any information it contains.

Acid-base equilibrium dynamics in methanol and dimethyl sulfoxide probed by two-dimensional infrared spectroscopy

Chiho Lee,[†] Hyewon Son,[†] and Sungnam Park^{†,§*}

[†]Department of Chemistry, Korea University, Seoul 136-701, Korea.

[§]Multidimensional Spectroscopy Laboratory, Korea Basic Science Institute, Seoul 136-713, Korea

* Author to whom correspondence should be addressed.

Email address: spark8@korea.ac.kr

ABSTRACT: Two-dimensional infrared (2DIR) spectroscopy, which has been proven to be an excellent experimental method for studying thermally-driven chemical processes, was successfully used to investigate an acid dissociation equilibrium of HN_3 in methanol (CH_3OH) and dimethyl sulfoxide (DMSO) for the first time. Our 2DIR experimental results indicate that the acid-base equilibrium occurs on picosecond timescales in CH_3OH but that it occurs on much longer timescales in DMSO. Our results imply that the different timescales of the acid-base equilibrium originate from different proton transfer mechanisms between the acidic (HN_3) and basic (N_3^-) species in CH_3OH and DMSO. In CH_3OH , the acid-base equilibrium is assisted by the surrounding CH_3OH molecules which can directly donate H^+ to N_3^- and accept H^+ from HN_3 and the proton migrates through the hydrogen-bonded chain of CH_3OH . On the other hand, the acid-base equilibrium in DMSO occurs through the mutual diffusion of HN_3 and N_3^- or direct proton transfer. Our 2DIR experimental results corroborate different proton transfer mechanisms in the acid-base equilibrium in protic (CH_3OH) and aprotic (DMSO) solvents.

Acid-base equilibria are ubiquitous in nature and play important roles in various chemical and biological systems. Under thermal equilibrium conditions, an acid (HA) dissociates into a proton (H^+) and its conjugate base (A^-) while the conjugate base is protonated to form HA. In buffered solutions, such an acid-base equilibrium is dynamic, which means that the deprotonation and protonation reactions occur equally and that equilibrium is maintained. From a kinetic viewpoint, how fast do the acid-base equilibrium dynamics occur in solutions? Is the acid-base equilibrium mechanistically different in different types of solvents? To answer these questions, the deprotonation ($HA \rightarrow H^+ + A^-$) and protonation ($H^+ + A^- \rightarrow HA$) rate constants need to be directly measured at equilibrium. However, direct measurements of the rate constants at equilibrium are quite challenging. In this work, two-dimensional infrared (2DIR) spectroscopy was used to study acid-base equilibrium dynamics by employing HN_3/N_3^- buffers in methanol (CH_3OH) and dimethyl sulfoxide (DMSO). 2DIR spectroscopy, which is an ultrafast vibrational analog of two-dimensional nuclear magnetic resonance (2D NMR), has been extensively used to elucidate fundamentally important molecular processes, such as, solute-solvent complexation,^{1, 2} carbon-carbon rotation,³ hydrogen-bond switching dynamics in aqueous solutions,⁴⁻⁸ ligand exchange,⁹ ion pair dimerization,¹⁰ ion pairing dynamics in electrolyte solutions,^{11, 12} intra- and intermolecular vibrational population dynamics¹³⁻¹⁹ and structural dynamics in solutions.^{20, 21}

Hydrazoic acid (HN_3) is a weak acid (i.e. $pK_a=4.7$ in water and $pK_a=8.9$ in CH_3OH) and is deprotonated to produce azide (N_3^-) in polar solvents.²² The asymmetric stretching vibration ($\nu_{N_3^-}$) of N_3^- is sensitive to its local environment and its frequency experiences a significant blue-shift when N_3^- is protonated to form HN_3 . FTIR spectra measured with HN_3/N_3^- buffers in CH_3OH and DMSO are shown in Figure 1(A). In both solvents, the low

frequency peaks ($\nu_{\text{N}_3^-}$) result from N_3^- and the high frequency peaks (ν_{HN_3}) from HN_3 in Figure 1(A) and they are spectrally well-distinguished. This spectral feature gives an opportunity to investigate the acid-base equilibrium by vibrationally probing the ν_{HN_3} and $\nu_{\text{N}_3^-}$ modes. The acid dissociation equilibrium of HN_3 in solutions is written as



where k_{depro} and k_{pro} are the deprotonation and protonation rate constants, respectively. At equilibrium, the deprotonation and protonation rates are equal (i.e., $k_{\text{depro}}[\text{HN}_3]=k_{\text{pro}}[\text{H}^+][\text{N}_3^-]$) and their ratio determines the acid dissociation constant ($k_{\text{depro}}/k_{\text{pro}}=[\text{H}^+][\text{N}_3^-]/[\text{HN}_3]=K_a$) in solutions. In addition, K_a can be readily determined by measuring the equilibrium concentrations of all the species. However, the experimental determination of the rate constants (k_{depro} and k_{pro}) in acid dissociation equilibria is not straightforward because the concentrations of acidic and basic species are time-independent after the equilibrium is established. Here, 2DIR spectroscopy was successfully used to directly study the acid dissociation equilibrium of HN_3 in CH_3OH and DMSO .

>> Figure 1 <<

Figure 1(B) and 1(C) display 2DIR spectra at $T_w=1$ and 25 ps measured with HN_3/N_3^- buffers in CH_3OH and DMSO . In CH_3OH , the red diagonal peaks at $(\omega_r=2132, \omega_i=2132)$ and $(\omega_r=2045, \omega_i=2045)$ in the 2DIR spectra are caused by the fundamental vibrational transitions ($\nu=0\rightarrow 1$) of ν_{HN_3} and $\nu_{\text{N}_3^-}$, respectively. The blue peaks below the diagonal peaks are from the $\nu=1\rightarrow 2$ transitions that are red-shifted along the ω_i axis by their vibrational anharmonicity. Similarly, in DMSO , the diagonal peaks at $(\omega_r=2125, \omega_i=2125)$ and $(\omega_r$

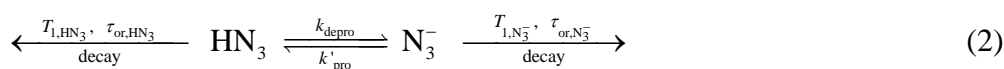
$\omega_i=2000$, $\omega_j=2000$) in the 2DIR spectra result from the $\nu=0\rightarrow 1$ transitions of ν_{HN_3} and $\nu_{\text{N}_3^-}$, respectively. In addition to the diagonal peaks resulting from HN_3 and N_3^- , the small peaks on the diagonal observed in DMSO originate from the aggregates of N_3^- there (See Figure S4 in the Electronic Supplementary Information). Most interestingly, cross-peaks appear in CH_3OH but are barely observed in DMSO when the 2DIR spectra at $T_w=25$ ps in Figures 1(B) and 1(C) are compared. In the case of HN_3/N_3^- buffers in CH_3OH , the cross-peaks in CH_3OH result directly from the deprotonation and protonation shown in Eq. (1). The 2DIR spectra in Figures 1(B) and 1(C) indicate that the deprotonation and protonation rates are much slower in DMSO than in CH_3OH . This is an interesting and important observation, which will be explained below by the different mechanisms of the deprotonation and protonation in CH_3OH and DMSO.

To quantitatively analyze the acid dissociation equilibrium of HN_3 in CH_3OH , we measured 2DIR spectra at a series of T_w and additionally performed polarization-controlled IR pump-probe (IR PP) experiments. Figure 2(A) displays T_w -dependent 2DIR spectra obtained with an HN_3/N_3^- buffer in CH_3OH . The 2DIR spectrum at each T_w is normalized by maximum peak amplitude for direct comparison of relative peak intensities. The T_w -dependent 2DIR spectra contain all the dynamic information on the molecular system under study. All the peaks in the 2DIR spectra decay with increasing T_w as a result of the vibrational population decay and orientational relaxation. First, the two diagonal peaks (HN_3 and N_3^-) are shown to be spectrally well separated as indicated in the 2DIR spectrum at $T_w=1.0$ ps. As T_w is increased, the N_3^- peak decays faster than the HN_3 peak. As shown in Figure 2(B), the population decay, $P(t)$, of HN_3 ($T_1=6.0$ ps) is slower than that of N_3^- ($T_1=3.0$ ps) while the orientational anisotropy decay, $r(t)$, of HN_3 ($\tau_{\text{or,avg}}=4.2$ ps) is faster than that of N_3^- ($\tau_{\text{or,avg}}=10.5$ ps). Overall, the population decay is the dominant contribution to the peak

decays in 2DIR spectra causing the N_3^- peak in the 2DIR spectra to decay much faster than the HN_3 peak as T_w is increased. It should be noted that N_3^- forms a stronger hydrogen-bond with CH_3OH and that its orientational relaxation is slower when compared with that of HN_3 . HN_3 has a shorter vibrational lifetime than N_3^- because the population decay of HN_3 occurs through an intermolecular vibrational energy transfer.¹⁸

>> Figure 2 <<

Most importantly, the cross-peaks in the 2DIR spectra grow gradually with the increases in T_w . As illustrated in the 2DIR spectrum at $T_w=25$ ps, the cross-peak in the upper left corner (indicated by the red arrow) results from the protonation of N_3^- ($H^+ + N_3^- \rightarrow HN_3$) while the cross-peak in the lower right corner (indicated by the blue arrow) results from the deprotonation of HN_3 ($HN_3 \rightarrow H^+ + N_3^-$). Therefore, the deprotonation and protonation rate constants (k_{depro} and k_{pro}) for the acid dissociation equilibrium in CH_3OH are readily determined by analyzing the cross-peak amplitudes as a function of T_w . By setting $k'_{pro}=k_{pro}[H^+]$ in Eq.(1), the acid dissociation equilibrium observed in the T_w -dependent 2DIR spectra can be described by the two-state exchange kinetic model,



where the two peaks associated with the acidic (HN_3) and basic (N_3^-) species exchange their populations with the deprotonation and protonation rate constants (k_{depro} and $k'_{pro}=k_{pro}[H^+]$), respectively, and the exchange rate constant is given by $k_{ex} = k_{depro}+k'_{pro}$. The equilibrium constant is given by $K'_a = k_{depro}/k'_{pro} \cong [N_3^-]/[HN_3]$. The individual peaks decay due to the vibrational population decay and orientational relaxation. The vibrational lifetimes ($T_{1,HN_3} = 6.0$ ps and $T_{1,N_3^-} = 3.0$ ps) and orientational relaxation times ($\tau_{or,HN_3} = 4.2$ ps and

$\tau_{\text{or},\text{N}_3^-} = 10.5 \text{ ps}$) for HN_3 and N_3^- were experimentally measured by polarization-controlled IR PP spectroscopy as shown in Figure 2(B). Additionally, the cross-peaks grow due to the deprotonation and protonation reactions. By using the two-state exchange kinetic model in Eq. (2), differential equations for the concentrations of individual peaks can be written and analytical solutions obtained (See the Electronic Supplementary Information). The analytical solutions represent the time-dependent changes of the concentrations of individual peaks and can be directly used to determine the deprotonation and protonation rate constants. A standard analytical method of T_w -dependent 2DIR spectra based on the two-state exchange kinetic model has been previously presented in great detail.^{11,12} Briefly, the individual peak volumes were obtained as plotted in Figure 2(C) by the 2D Gaussian peak fitting method because the volumes of the individual peaks in the 2DIR spectrum were directly proportional to their concentrations.^{11,12} The analytical solution for the two-state exchange kinetic model was fitted to the plot of the peak volumes against T_w as shown in Figure 2(C).^{11,12} From the two-state exchange kinetic analyses, the deprotonation and protonation rate constants were determined to be $k_{\text{depro}} = (180 \pm 20 \text{ ps})^{-1}$ and $k'_{\text{pro}} = k_{\text{depro}}/K'_a = (80 \pm 10 \text{ ps})^{-1}$, respectively, and the exchange rate constant obtained was $k_{\text{ex}} = k_{\text{depro}} + k'_{\text{pro}} = (55 \pm 10 \text{ ps})^{-1}$, which corresponds to the rate constant of the cross-peak growth in T_w -dependent 2DIR spectra.

In the case of HN_3/N_3^- buffers in DMSO, the cross-peaks in the 2DIR spectra are barely observed as shown in Figure 1(B). In general, the dynamic range of 2DIR spectroscopy is limited by the lifetimes of vibrational probes. In other words, chemical exchange processes which have the timescales much longer than the lifetimes of vibrational probes cannot be exactly measured by 2DIR spectroscopy. The 2DIR spectra measured with HN_3/N_3^- buffers in DMSO shown in Figure 2(C) imply that the deprotonation and protonation reactions in DMSO would rather occur on a much longer timescale than the vibrational lifetimes of ν_{HN_3}

and $\nu_{\text{N}_3^-}$ modes and thus the deprotonation and protonation reactions are not observed in our experimental time range. Accordingly, the deprotonation and protonation rate constants were not able to be exactly determined for HN_3/N_3^- buffers in DMSO. However, our 2DIR experimental results indicate that the timescale of the acid dissociation equilibrium is substantially longer in DMSO than in CH_3OH .

It is very intriguing to find that the acid dissociation equilibrium of HN_3 occurs on a picosecond timescale in CH_3OH but on a much longer timescale in DMSO. In our experiments, the concentrations of HN_3 (0.24 M in CH_3OH and 0.30 M in DMSO) and N_3^- (0.10 M in methanol and 0.06 M in DMSO) are relatively low in the two solvents, which indicates that there are ~ 65 solvent molecules per solute in CH_3OH and ~ 35 solvent molecules per solute in DMSO. Under this condition, it is considered unlikely that HN_3 and N_3^- forms an encounter complex (i.e., $\text{N}_3\text{H}\cdots\text{N}_3^-$) in CH_3OH and DMSO. A direct proton transfer between HN_3 and N_3^- within the encounter complex (i.e., $\text{N}_3\text{H}\cdots\text{N}_3^- \rightarrow \text{N}_3^-\cdots\text{HN}_3$) is assumed to be negligible. A plausible explanation for different timescales of the acid-base equilibrium in CH_3OH and DMSO is given in the following. CH_3OH ($pK_a=15.5$) is a protic solvent capable of donating H^+ to N_3^- and accepting H^+ from HN_3 . On the other hand, DMSO (dimethyl sulfoxide, $pK_a\sim 35$) is an aprotic solvent which is largely incapable of donating H^+ . These different properties of the two solvents would provide different mechanistic pathways for the acid-base equilibrium. In CH_3OH , the deprotonation and protonation for the acid-base equilibrium can be assisted by the surrounding hydrogen-bonded methanol molecule. HN_3 is deprotonated to CH_3OH to which HN_3 is directly hydrogen-bonded ($\text{CH}_3\text{OH}\cdots\text{HN}_3 \rightarrow \text{CH}_3\text{OH}_2^+\cdots\text{N}_3^-$). In a similar way, N_3^- is protonated by CH_3OH to which N_3^- is directly hydrogen-bonded ($\text{CH}_3\text{OH}\cdots\text{N}_3^- \rightarrow \text{CH}_3\text{O}^-\cdots\text{HN}_3$). The proton (H^+) migrates through a hydrogen-bonded chain of CH_3OH as illustrated in Figure 3. In fact, Morrone and Tuckerman carried out *ab initio* molecular dynamics simulations with an excess proton in CH_3OH to

study the proton transfer mechanism in CH_3OH .²³ They found that the excess proton migrates in a random fashion along a relatively long chain of hydrogen-bonded CH_3OH . In short, both deprotonation and protonation for the acid-base equilibrium in CH_3OH are assisted by the surrounding CH_3OH molecules and the hydrogen-bonded network of CH_3OH forms an efficient proton transfer channel between HN_3 and N_3^- facilitating the deprotonation and protonation.

>> Figure 3 <<

On the other hand, DMSO can accept a proton but can rarely donate one ($pK_a \sim 35$ for DMSO). In addition, DMSO cannot form efficient chains for proton migration, as shown in CH_3OH . To complete the deprotonation and protonation reactions in an acid-base equilibrium, the proton has to migrate directly from HN_3 to N_3^- or HN_3 and N_3^- need to diffuse mutually through the solvent matrix to form an encounter complex and subsequently the proton transfer takes place within the encounter complex. For the acid-base equilibrium in DMSO, the mutual diffusion of HN_3 and N_3^- or the proton migration through the solvent matrix would be very slow. As a consequence, the deprotonation and protonation rates were observed to be much slower in DMSO than in CH_3OH .

In conclusion, we comparatively studied the acid dissociation equilibrium of HN_3 in CH_3OH and DMSO by 2DIR spectroscopy. The acid-base equilibria in CH_3OH and DMSO, which were found to occur on much different timescales, were explained by fundamentally different proton transfer mechanisms. Our experimental results provide some insight into different proton transfer mechanisms for the acid-base equilibria in protic and aprotic solvents. The acid-base equilibrium in protic solvents (i.e., CH_3OH) is assisted by the neighboring solvent and its hydrogen-bonded chain while the acid-base equilibrium occurs in

aprotic solvents (i.e., DMSO) by the mutual diffusion of acidic and basic species and/or direct proton migration. Therefore, the acid-base equilibrium is much faster in protic solvents than in aprotic solvents. Solvent-dependent acid-base equilibrium dynamics may play an important role in determining the rates of chemical reactions involving the proton transfer occurring in protic and aprotic solvents. In addition, our experimental results are conceptually important and can be used to understand the acid-base equilibria in various chemical and biochemical systems.

Experimental method

NaN_3 , methanol (CH_3OH), dimethyl sulfoxide (DMSO), and anhydrous sulfuric acid were purchased from Sigma-Aldrich. To prepare the sample solutions, NaN_3 salt was dissolved in methanol and DMSO, and then anhydrous sulfuric acid was added. Upon addition of anhydrous sulfuric acid, $\text{Na}_2\text{SO}_4(\text{s})$ was precipitated because of its low solubility in both solvents. $\text{Na}_2\text{SO}_4(\text{s})$ was separated from the solutions by centrifugation. HN_3/N_3^- buffers in methanol and DMSO were prepared as $[\text{HN}_3]/[\text{N}_3^-]=0.24 \text{ M}/0.10 \text{ M}$ in methanol and $[\text{HN}_3]/[\text{N}_3^-]=0.30 \text{ M}/0.06 \text{ M}$ in DMSO. The sample solution was housed in a home-made IR cell with two CaF_2 windows (3 mm thick) and a 12 μm thick Teflon spacer. The FTIR spectra of the sample solutions were measured at 22 $^\circ\text{C}$.

Experimental details on polarization-controlled IR PP and 2DIR spectroscopy have been presented and discussed elsewhere.²⁴⁻²⁶ Briefly, a ~ 60 fs mid-IR pulse centered at $\sim 2100 \text{ cm}^{-1}$ was used for 2DIR and IR PP experiments. In 2DIR spectroscopy, three mid-IR pulses were focused onto the sample and their relative time-delays were controlled.²⁵ The signal was emitted from the sample in a new phase-matched direction and was heterodyned by a local oscillator. The 2DIR signals were collected by scanning the τ -axis at a fixed T_w and were frequency-resolved through the spectrometer with a 64-element HgCdTe (MCT) array

detector obtaining temporal interferograms as a function of τ at the emission frequencies (ω). Numerical Fourier transformation of the temporal interferograms along the τ -axis gave the excitation frequency axis (ω_τ). 2DIR spectrum at a given T_w was displayed with the excitation (ω_τ) and emission (ω) frequencies. The 2DIR spectra were obtained at a series of T_w . For polarization-controlled IR PP experiments, the pump beam was vertically polarized and the polarization of the probe beam was set to 45 degrees with respect to that of the pump beam.²⁷ The probe beam was collimated after the sample and went through an analyzer polarizer which was mounted on a motorized rotational stage. The IR PP signals were frequency-resolved. The parallel and perpendicular IR PP signals were obtained alternately by rotating the analyzer polarizer in such a way that the polarization of the signal was set to be vertical and horizontal with respect to the polarization of the pump beam. The 2DIR and IR PP experiments were conducted at 22 °C.

Acknowledgements

This work was supported by National Research Foundation of Korea (NRF) grants funded by the Korean government (MEST) (Nos. 2013R1A1A2009991 and 20100020209) and a KETEP grant (No. 20104010100640). The 2DIR and IR pump-probe experiments were performed in the Multidimensional Spectroscopy Laboratory at the Korea Basic Science Institute (KBSI), Seoul Center.

References

1. J. Zheng, K. Kwak, J. Asbury, X. Chen, I. Piletic and M. D. Fayer, *Science*, 2005, 309, 1338-1343.
2. Y. S. Kim and R. M. Hochstrasser, *Proc. Natl. Acad. Sci. U.S.A.*, 2005, 102, 11185-11190.
3. J. Zheng, K. Kwak, J. Xie and M. D. Fayer, *Science*, 2006, 313, 1951-1955.
4. S. Park, M. Odelius and K. J. Gaffney, *J. Phys. Chem. B.*, 2009, 113, 7825-7835
5. D. E. Moilanen, D. Wong, D. E. Rosenfeld, E. E. Fenn and M. D. Fayer, *Proc. Natl. Acad. Sci. U.S.A.*, 2009, 106, 375-380.
6. M. Ji, M. Odelius and K. J. Gaffney, *Science*, 2010, 328, 1003.
7. R. A. Nicodemus, K. Ramasesha, S. T. Roberts and A. Tokmakoff, *J. Phys. Chem. Lett.*, 2010, 1, 1068-1072.
8. H. Son, D. Nam and S. Park, *J. Phys. Chem. B*, 2013, 117, 13604-13613.
9. S. Park, M. Ji and K. J. Gaffney, *J. Phys. Chem. B*, 2010, 114, 6693-6702.
10. M. Ji, S. Park and K. J. Gaffney, *J. Phys. Chem. Lett.*, 2010, 1, 1771-1775.
11. K.-H. Park, S. R. Choi, J.-H. Choi, S. Park and M. Cho, *ChemPhysChem*, 2010, 11, 3632-3637.
12. K.-K. Lee, K.-H. Park, D. Kwon, J.-H. Choi, H. Son, S. Park and M. Cho, *J. Chem. Phys.*, 2011, 134, 064506.
13. M. J. Nee, C. R. Baiz, J. M. Anna, R. McCanne and K. J. Kubarych, *J. Chem. Phys.*, 2008, 129, 084503.
14. H. T. Bian, J. B. Li, X. W. Wen and J. R. Zheng, *J. Chem. Phys.*, 2010, 132.
15. S. Park and M. Ji, *ChemPhysChem*, 2011, 12, 799-805.
16. J. M. Anna, J. T. King and K. J. Kubarych, *Inorg. Chem.*, 2011, 50, 9273-9283.

17. J. Borek, F. Perakis, F. Kläsi, S. Garrett-Roe and P. Hamm, *J. Chem. Phys.*, 2012, 136, 224503.
18. H. Son, K.-H. Park, K.-W. Kwak, S. Park and M. Cho, *Chem. Phys.*, 2013, 422, 37-46.
19. H. Chen, X. Wen, X. Guo and J. Zheng, *Phys. Chem. Chem. Phys.*, 2014, 16, 13995-14014.
20. D. B. Strasfeld, Y. L. Ling, S.-H. Shim and M. T. Zanni, *J. Am. Chem. Soc.*, 2008, 130, 6698–6699.
21. K. Adamczyk, M. Candelaresi, R. Kania, K. Robb, C. Bellota-Anto'n, G. M. Greetham, M. R. Pollard, M. Towrie, A. W. Parker, P. A. Hoskisson, N. P. Tucker and N. T. Hunt, *Phys. Chem. Chem. Phys.*, 2012, 14, 7411-7419.
22. B. W. Clare, D. Cook, E. C. F. Ko, Y. C. Mac and A. J. Parker, *J. Am. Chem. Soc.*, 1966, 88, 1911-1916.
23. J. A. Morrone and M. E. Tuckerman, *J. Chem. Phys.*, 2002, 117, 4403-4413.
24. M. Khalil, N. Demirdoeven and A. Tokmakoff, *J. Phys. Chem. A*, 2003, 107, 5258-5279.
25. S. Park, K. Kwak and M. D. Fayer, *Laser Phys. Lett.*, 2007, 4, 704-718.
26. P. Hamm and M. Zanni, *Concepts and Methods of 2D Infrared Spectroscopy* Cambridge University Press, UK, 2011.
27. S. Park and M. D. Fayer, *Proc. Natl. Acad. Sci. USA*, 2007, 104, 16731-16738.

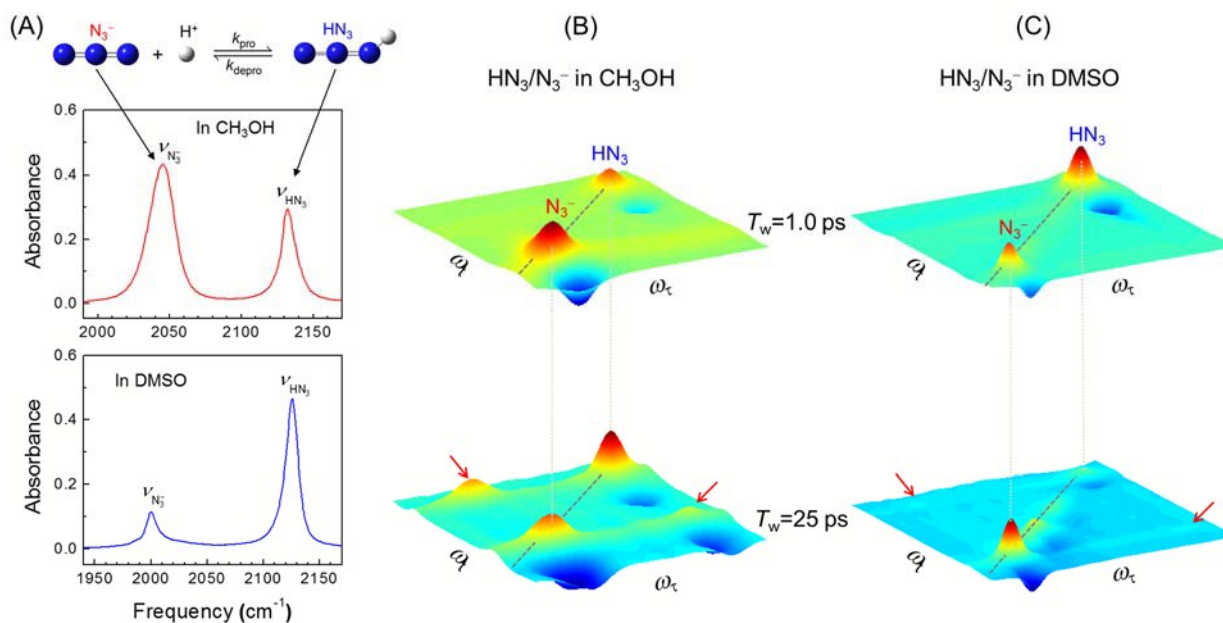


Figure 1. (A) FTIR spectra measured with an HN_3/N_3^- buffer in CH_3OH and DMSO. N_3^- peaks at the low frequency ($\nu_{N_3^-}$) while HN_3 peaks at the high frequency (ν_{HN_3}). (B) and (C) 2DIR spectra measured with an HN_3/N_3^- buffer in CH_3OH and DMSO. The 2DIR spectrum at a given T_w is normalized by the maximum peak amplitude. The diagonal axis is indicated by a dashed line on each 2DIR spectrum. In CH_3OH , the cross-peaks are indicated by arrows and their amplitudes grow at $T_w=25$ ps. In DMSO, the cross-peaks are barely observed.

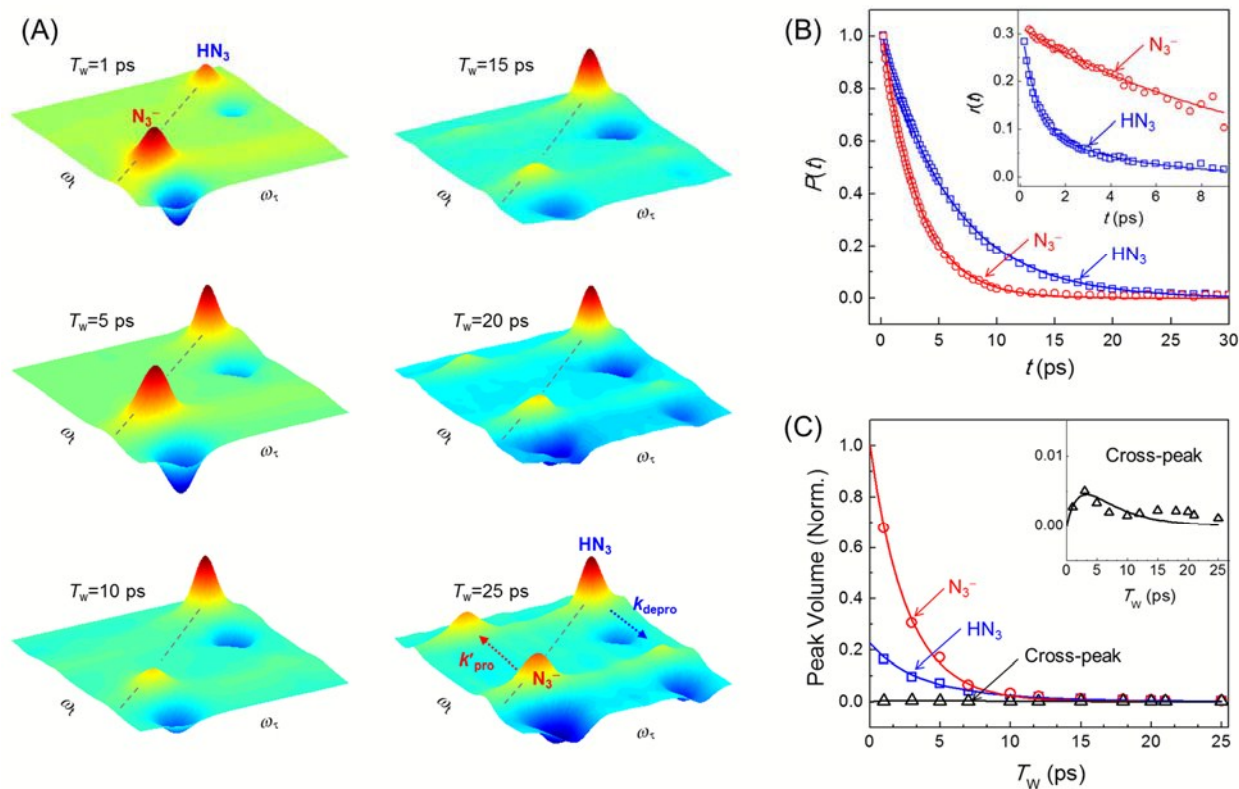


Figure 2. (A) 2DIR spectra measured at a series of T_w with an HN_3/N_3^- buffer in CH_3OH . The 2DIR spectra are normalized at the peak maximum. The cross-peaks result from deprotonation ($\text{HN}_3 \rightarrow \text{H}^+ + \text{N}_3^-$) and protonation ($\text{H}^+ + \text{N}_3^- \rightarrow \text{HN}_3$) as shown in the 2DIR spectrum at $T_w = 25$ ps. (B) The population decays, $P(t)$, and orientational anisotropy decay, $r(t)$, of HN_3 and N_3^- were measured by polarization-controlled IR PP spectroscopy. (C) The volumes of the diagonal peaks and cross-peaks in the 2DIR spectra are plotted as a function of T_w (data points). The solid lines are the fit by the analytical solutions obtained from the two-state exchange kinetic model. The inset shows the cross-peak volumes as a function of T_w .

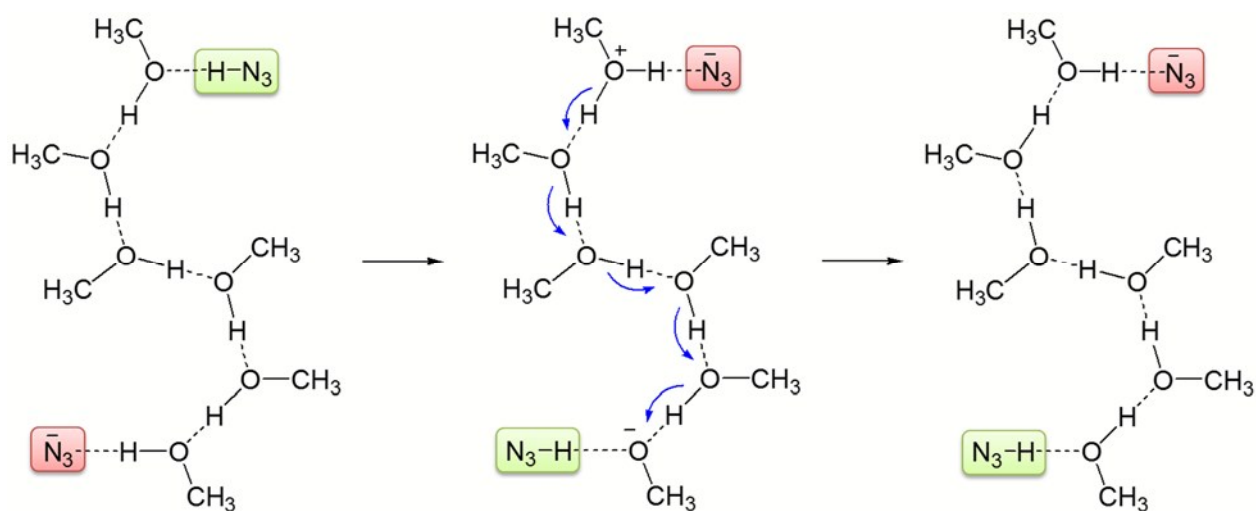


Figure 3. Illustration of the proton transfer mechanism for the acid-base equilibrium occurring in CH_3OH . In CH_3OH , HN_3 is deprotonated by a hydrogen-bonded CH_3OH and N_3^- is protonated by a hydrogen-bonded CH_3OH . The proton migrates through the hydrogen-bonded chain of CH_3OH . This proton transfer mechanism was proposed from the results of the ab initio molecular dynamics simulation in Ref. 23.